The Mairan domes: Silicic volcanic constructs on the Moon

Timothy D. Glotch,[1] Justin J. Hagerty,[2] Paul G. Lucey,[3] B. Ray Hawke,[3] Thomas A. Giguere,[3] Jessica A. Arnold,[1] Jean-Pierre Williams,[4] Bradley L. Jolliff,[5] and David A. Paige[4]

Received 2 September 2011; revised 19 October 2011; accepted 19 October 2011; published 15 November 2011.

[1] The Mairan domes are four features located in northern Oceanus Procellarum at ~312.3E, 41.4N on the Moon. High resolution visible imagery, visible-to-mid-IR spectra, and Lunar Prospector Th abundance data all indicate that these four domes have a composition that is consistent with derivation from a Si-rich, highly evolved magma. **Citation:** Glotch, T. D., J. J. Hagerty, P. G. Lucey, B. R. Hawke, T. A. Giguere, J. A. Arnold, J.-P. Williams, B. L. Jolliff, and D. A. Paige (2011), The Mairan domes: Silicic volcanic constructs on the Moon, *Geophys. Res. Lett.*, *38*, L21204, doi:10.1029/2011GL049548.

1. Introduction

[2] The Mairan domes are four distinct features at the northern edge of Oceanus Procellarum, centered at ~312.3E, 41.4 N, west of Mairan crater and east of the Rümker hills. These domes have relatively high albedos and unique morphological and spectral characteristics. *Scott and Eggleton* [1973], using Earth-based photographs and Lunar Orbiter data, mapped the three northern domes as volcanic cumulo-domes and interpreted them to have been formed by viscous felsic lava. *Head and McCord* [1978] used Earth-based telescopic multispectral images to show that the three southern domes are spectrally anomalous compared to surrounding mare and highlands material, with strong ultraviolet absorptions that are responsible for their red color. They noted that the Mairan domes are similar in shape and surface texture to many terrestrial domes of dacitic and rhyolitic composition formed by extrusions of viscous lavas at low rates. *Wilson and Head* [2003] used the basic morphologic and morphometric characteristics of the domes as a basis for estimation of their yield strength, plastic viscosity, and eruption rates and duration. The results of their calculations confirmed previous suggestions that they were formed from magmas with substantially higher viscosity than those typical of mare basalts. A fourth dome, northwest of these three, was mapped by *Scott and Eggleton* [1973] as a volcanic dome, and is described in detail here for the first time.

[3] Recent results from the Diviner Lunar Radiometer Experiment on board the Lunar Reconnaissance Orbiter have shown that some other dome-shaped features on the Moon exhibit infrared spectra consistent with highly silicic compositions [*Glotch et al.*, 2010; *Greenhagen et al.*, 2010; *Jolliff et al.*, 2011]. These features, which include the Gruithuisen domes, Hansteen alpha, and the Compton Bel'kovich anomaly, also exhibit strong Th anomalies in Lunar Prospector (LP) Gamma Ray Spectrometer (GRS) data, suggesting that they formed from highly evolved magmas [*Lawrence et al.*, 2003, 2005; *Hagerty et al.*, 2006]. In this work, we synthesize data from Diviner, SELENE Spectral Profiler (SP), Chandrayaan-1 Moon Mineralogy Mapper (M^3), GRS, and high resolution Lunar Reconnaissance Orbiter Camera (LROC) Narrow Angle Camera (NAC) images to demonstrate that the Mairan domes are silicic volcanic constructs.

2. Data and Methods

[4] For this study, we used Diviner data acquired between July, 2009 and April, 2011. To achieve the best signal to noise and to avoid spurious effects due to high emission angle observations, we only used data acquired between 10 am and 2 pm local time with emission angles of <8°. Data were binned at 128 pixels per degree, and Diviner concavity index maps and emissivity data products were produced in the same manner as *Glotch et al.* [2010]. Other details of Diviner data acquisition and processing are available in the auxiliary material.[1]

[5] We used the M^3 data strip M3G20090209T072710 that fully covers the Mairan domes. It has a spatial resolution of 140 m/pix and 85 bands with spectral resolution ranging from 20 nm to 40 nm. The radiance data were converted to apparent reflectance using a solar spectrum convolved to M^3 global mode spectral bands (available at http://m3.jpl.nasa.gov/m3data.html). While the hyperspectral image is useful to display spectral variance across the scene, individual spectra from this particular image are quite noisy. These Level 1b data use a preliminary calibration, and the noise should be significantly reduced with the final Level 2 calibration [*Green et al.*, 2011]. To investigate the detailed VNIR spectral properties of these features, we used data from SP [*Matsunaga et al.*, 2008]. Spectra were extracted from revolutions 1733, 2401, 3568, 4566, 6089, and 7137.

[6] To facilitate analysis of the low spatial resolution GRS data, we conducted forward modeling to effectively increase

[1]Department of Geological Sciences, Stony Brook University, Stony Brook, New York, USA.
[2]Astrogeology Science Center, U.S. Geological Survey, Flagstaff, Arizona, USA.
[3]Hawaii Institute of Geophysics and Planetology, University of Hawaii at Manoa, Honolulu, Hawaii, USA.
[4]Department of Earth and Space Sciences, University of California, Los Angeles, California, USA.
[5]Department of Earth and Planetary Sciences, Washington University in St. Louis, St. Louis, Missouri, USA.

0094-8276/11/2011GL049548

[1]Auxiliary materials are available in the HTML. doi:10.1029/2011GL049548.

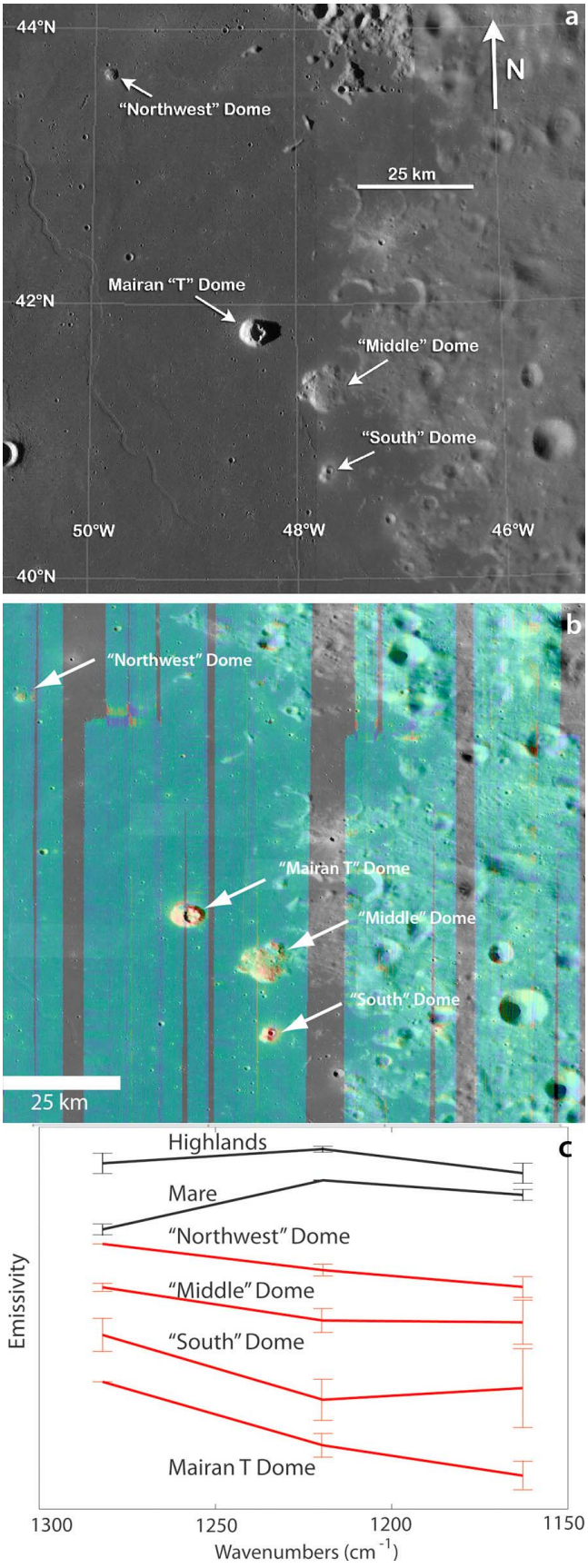

the resolution by allowing compositional estimation of individual geologic units on the lunar surface [e.g., *Lawrence et al.*, 2005; *Hagerty et al.*, 2006]. The forward modeling techniques combine sample-based data, morphologic data, and data from orbital remote sensing missions to obtain information about the elemental abundances of geologic features that are at or smaller than the spatial resolution of the LP data. Additional details of this process are available in the auxiliary material.

[7] Lunar Reconnaissance Orbiter Camera (LROC) Wide Angle Camera (WAC) images (100 m/pixel) and Narrow Angle Camera (NAC) images (0.5 to 1.5 m/pixel) were used to investigate the geology, morphology, and surface roughness of the Mairan domes [*Robinson et al.*, 2010]. Topographic data for the Mairan domes were provided by the WAC-derived digital terrain model (DTM) at the 100 m/pixel scale [*Scholten et al.*, 2010] and a NAC-derived DTM for the Mairan T dome [*Tran et al.*, 2011].

3. Results

[8] A concavity index map based on the three "8 μm" channels of Diviner is shown in Figure 1a. This map clearly shows that the four dome features (marked by white arrows) have higher index values than the surrounding terrain. High concavity index values are marked by the red and yellow colors on the map and are confined to the three domes described by *Head and McCord* [1978] and *Wilson and Head* [2003] and the fourth, northern-most dome, mapped by *Scott and Eggleton* [1973]. As discussed by *Glotch et al.* [2010], few minerals have the concave up spectral shape required to produce the red colors seen in Figure 1b. They include quartz and other SiO_2 polymorphs, K-feldspars and plagioclase feldspars more sodic than labradorite. Although the detailed mineralogy cannot be determined from the three-point Diviner spectra, these classes of minerals are consistent with extrusive silicic lavas.

[9] Representative spectra of each of the domes, the surrounding mare, and the highlands are shown in Figure 1b. We employed a simple linear mixing model using quartz as one end-member and augite, anorthite, or microcline as the second end-member in addition to a blackbody spectrum to place a broad constraint on the compositions of the domes. Details of the model are available in the auxiliary material. The spectra of three of the domes can be modeled with 0.00% RMS error using only two end-members (Table 1). The percentage of quartz for these three models ranges from ~30% to 90%. The Mairan "south" dome is modeled as 100% quartz with no additional components, but has an RMS error of 0.214%. This is due to the fact that the Mairan "south" spectrum has a higher band5/band4 emissivity ratio than our library quartz end-member spectrum. For each of these models, quartz can be taken as a proxy for any SiO_2 phase, including cristobalite or tridymite, which are more likely

Figure 1. (a) LROC WAC regional context image. (b) Overlay of Diviner concavity index parameter on portion of the LROC WAC global mosaic. Diviner data are stretched from concavity index values of −0.025 (blue) to 0.015 (red). (c) Whole-dome Diviner spectra extracted from each of the domes and representative spectra of the surrounding mare and highlands.

Table 1. Deconvolution Results of Diviner 3-Point Spectra Covering the Mairan Domes and Modeled Th Abundances

	Northwest	Mairan T Dome	Mairan "Middle"	Mairan "South"
		Model 1		
Quartz	28%	31%	70%	100%
Augite	72%	69%	30%	0%
% RMS	0.00	0.00	0.00	0.214
		Model 2		
Quartz	30%	42%	91%	100%
Anorthite	70%	58%	9%	0%
% RMS	0.00	0.00	0.00	0.214
		Model 3		
Quartz	0%	0%	73%	100%
Microcline	100%	100%	27%	0%
%RMS	0.145	0.181	0.00	0.214
Th (ppm)	8.8 ± 3	36.5 ± 9	48.0 ± 6	82.8 ± 19

to occur in extrusive settings [e.g., *Robinson and Taylor*, 2011]. Because we have only three spectral bands to work with, the spectral unmixing problem is poorly constrained, and the results of these models should not be taken as absolute. Rather, the results can be used to gage the relative differences in composition between the domes, highlands, and mare.

[10] Our GRS modeling (Figure 2) indicates that the four domes (northwest, Mairan T, middle, and south) have optimum Th values of 8.8 ± 3 ppm, 36.5 ± 9 ppm, 48.0 ± 6 ppm, and 82.8 ± 19 ppm, respectively. The domes also have FeO abundances ranging from 6–10 wt.% FeO, based on Clementine multispectral imagery [*Lucey et al.*, 2000]. When compared to values in the lunar sample suite these Th and FeO values are consistent with alkali-suite lithologies such as granites, felsites, and quartz monzodiorites [i.e., *Jolliff*, 1998; *Korotev*, 1998; *Papike et al.*, 1998]. These Th values are also consistent with terrestrial rhyolites that occur as bi-modal pairings with basalts. The results for the Mairan domes are consistent with investigations of similar features such as the Gruithuisen domes, the Lassel massif, Hansteen alpha, and Compton-Bel'kovich [*Hawke et al.*, 2003; *Hagerty et al.*, 2006; *Glotch et al.*, 2010; *Jolliff et al.*, 2011].

[11] Figure 3a shows a mosaic of NAC images of the Mairan T dome which is nearly circular in planform. The diameter of this volcanic construct ranges between 6.6 and 7.1 km and it rises to a maximum height of 771 m above the surrounding mare surface. Since the Mairan T dome is clearly embayed by much younger mare deposits, its original height could have been considerably greater. The steep slopes on the flank range from 22° to 27° and have a well-defined contact with the mare [*Tran et al.*, 2011]. These flank slope values are in the same range as those exhibited for other steep-sided silicic domes such as Gruithuisen NW (22°–27°) and Compton-Bel'kovich dome 1 (20°–26°) [*Tran et al.*, 2011; *Jolliff et al.*, 2011]. Mairan T crater occupies the summit area of the dome and has an irregular shape. While early workers considered Mairan T to be a single, irregular crater [*Andersson and Whitaker*, 1982], Figure 3a clearly shows that the depression is composed of a series of smaller coalesced craters. Mairan T is roughly 3.8 km wide and up to 450 m deep [*Tran et al.*, 2011]. The slope of the walls of the depression ranges from 13° to 25°. Most of the major block concentrations on the dome are associated with the steep walls and rim of the Mairan T depression (Figure 3a). The morphologies of the craters that make up the Mairan T depression indicate an internal

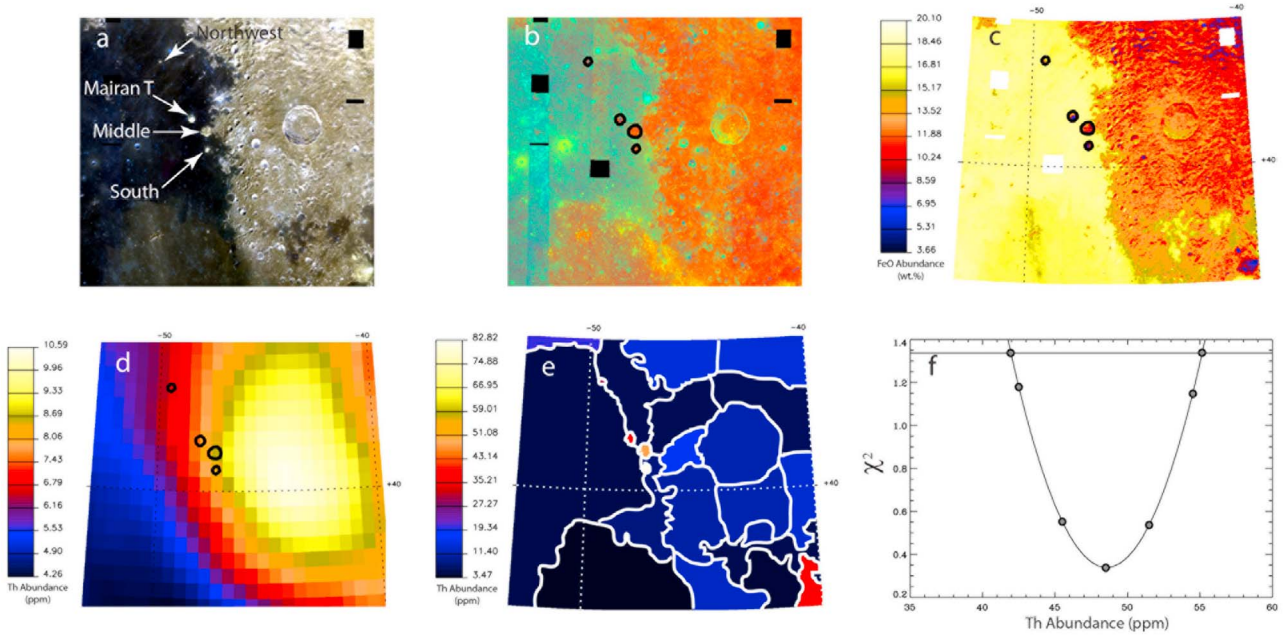

Figure 2. (a) Clementine "true color" albedo image of the Mairan domes. (b) Clementine color ratio map of the domes (outlined in black). (c) Clementine FeO map of the domes. The domes have between 6 and 10 wt.% FeO based on *Lucey et al.*'s [2000] algorithm. (d) GRS Th map (0.5° × 0.5°) of the domes (outlined in black). Without process refinement, the domes appear to have between 7 and 9 ppm Th. (e) Individual features in the scene chosen for forward modeling. (f) Chi-squared error analysis of the middle dome, indicating that the optimum Th value for the dome is 48 ± 6 ppm Th.

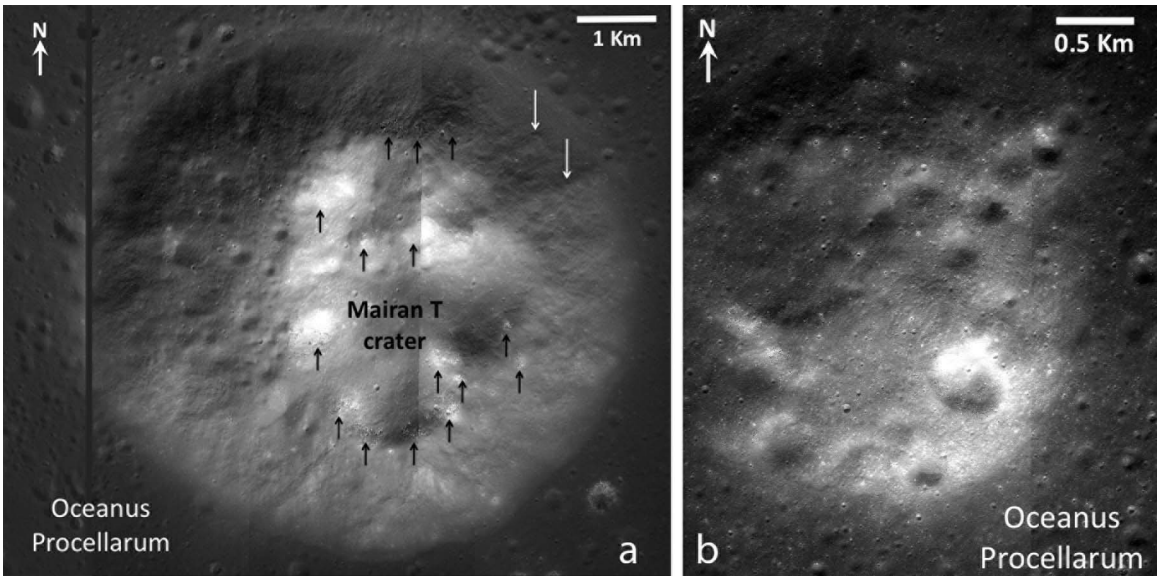

Figure 3. LROC NAC mosaics of two Mairan domes. (a) Mairan T crater and dome. The mosaic comprises three pairs of NAC images (M120169033, M127247376, M140215754) and has a resolution of 0.8 m/pixel. Black arrows indicate areas with high block densities and white arrows point to two of several ridges that may be associated with viscous lava flows. (b) NW Mairan dome. The mosaic is made up of the M124899196 left and right images and has a resolution of 0.8 m/pixel.

origin, likely formed by collapse associated with magma withdrawal [*Scott and Eggleton*, 1973]. The surface of the Marian T dome is rough at a variety of scales, and several ridges can be seen in Figure 3a that extend from the summit depression to the bottom of the dome. These ridges may be associated with viscous lava flows.

[12] A mosaic of NAC images of the NW Mairan dome is shown in Figure 3b. The feature is ~3.2 km in diameter and is roughly circular. The surface is generally rough, but the slopes of the NW dome are shallower than those of the Mairan T dome and it rises to a maximum height of only 186 m above the surrounding younger mare basalts. Similar to the Mairan T dome, the original height was likely greater, although based on the isopach map of *De Hon* [1979], the heights of the domes could not have been more than 250 m greater than we see today.

[13] M^3 and SP data are consistent with a silicic composition for the domes. As would be expected for silicic features, the NIR data show only weak ferrous iron absorptions in the 1 and 2 μm regions (auxiliary material). In general, the NIR is insensitive to Fe-free minerals, so the lack of strong bands in the SP are consistent with the presence of abundant Fe-free minerals such as quartz. Fe-bearing plagioclase has a broad, weak feature near 1250 nm, which may be present in some of the spectra (auxiliary material). Finally, the spectra covering the domes have much higher overall reflectance values than the surrounding terrain, suggesting a lack of dark, mafic minerals, and the presence of bright, silicic minerals.

4. Discussion

[14] As shown in Figure 1b and Table 1, the four domes exhibit different Diviner spectra and derived mineralogy. This is at least partly due to lateral mixing between the silicic material associated with the domes and the surrounding mare material, although differences in primary dome composition cannot be ruled out. The silicic nature of the domes, as well as their variable compositions, is supported by GRS Th data. The estimated Th contents and the modeled quartz abundances from Diviner data track exactly with each other (Table 1). The modeled Th content of the south dome ~83 ppm is higher than is seen in any Apollo felsite sample. This is likely because the modeled abundance was confined to the geographic limits of the dome, while small, fresh craters on the dome have distributed Th-bearing material onto the plains near the dome. The result is a modeled Th content that is likely higher than the true value. Diviner and GRS Th data are supported by SP VNIR spectra, which have only weak features due to low-Ca pyroxene and glass. These spectra are consistent with a large portion of spectrally neutral material such as quartz or other SiO_2 polymorphs. The conclusion from spectral data that the domes have a silicic composition is also supported by high resolution imagery and LROC-derived topography. The domes' rugged appearance in LROC narrow angle imagery and steep slopes are consistent with formation from viscous lava such as rhyolite, dacite, or basaltic andesite [*Wilson and Head*, 2003].

5. Conclusions

[15] We have applied a variety of remote sensing techniques—VNIR through mid-IR spectroscopy, Th abundance modeling, and high resolution topography and imaging—to the lunar Mairan domes. This integrated approach leads to the robust conclusion that the four Mairan domes formed as the result of silicic volcanism. Clear examples of extrusive silicic materials (crystobalite or trydimite-bearing rather than quartz-bearing) are rare in the Apollo sample collection [*Robinson and Taylor*, 2011], and the question of the genesis of magma that resulted in these features is unsettled, with both silicate liquid immiscibility and basaltic underplating proposed as potential mechanisms [*Jolliff et al.*,

1999; *Hagerty et al.*, 2006]. Recent results [*Glotch et al.*, 2010; *Jolliff et al.*, 2011] have shown that highly silicic lunar rocks are clearly more volumetrically important in the lunar crust than is evident from the Apollo sample suite. Sample return from the Mairan domes or other highly silicic lunar features would help to settle this question of their origin and fill a major gap in our understanding of late stage magmatic evolution on the Moon.

[16] **Acknowledgments.** This work was supported by Lunar Reconnaissance Obiter Participating Scientist Program grant # NNX08AM78G made to TDG. Portions of this work conducted by J.J. Hagerty were supported by NASA through Planetary Mission Data Analysis Program grant NNH09AL42I (JJH, PI) and were conducted under the auspices of the U. S. Department of the Interior. We thank Jeff Taylor, Katie Robinson, and Sam Lawrence, who provided valuable comments on an early version of the manuscript, and Noah Petro and Peter Isaacson, who provided detailed formal reviews that improved the content and clarity of the paper.

[17] The Editor thanks Noah Petro and Peter Isaacson for their assistance in evaluating this paper.

References

Andersson, L. E., and E. A. Whitaker (1982), *The NASA Catalog of Lunar Nomenclature*, *NASA Ref. Publ.*, 1097, 183 pp.

De Hon, R. A. (1979) Thickness of the western mare basalts, *Lunar Planet. Sci. Conf.*, *10th*, 2935–2955.

Glotch, T. D., et al. (2010), Highly silicic compositions on the Moon, *Science*, *329*, 1510–1513, doi:10.1126/science.1192148.

Green, R. O., et al. (2011), The Moon Mineralogy Mapper (M3) imaging spectrometer for lunar science: Instrument description, calibration, on-orbit measurements, science data calibration and on-orbit validation, *J. Geophys. Res.*, *116*, E00G19, doi:10.1029/2011JE003797.

Greenhagen, B. T., et al. (2010), Global silicate mineralogy of the Moon from the Diviner Lunar Radiometer, *Science*, *329*, 1507–1509, doi:10.1126/science.1192196.

Hagerty, J. J., D. J. Lawrence, B. R. Hawke, D. T. Vaniman, R. C. Elphic, and W. C. Feldman (2006), Refined thorium abundances for lunar red spots: Implications for evolved, nonmare volcanism on the Moon, *J. Geophys. Res.*, *111*, E06002, doi:10.1029/2005JE002592.

Hawke, B. R., D. J. Lawrence, D. T. Blewett, P. G. Lucey, G. A. Smith, P. D. Spudis, and G. J. Taylor (2003), Hansteen Alpha: A volcanic construct in the lunar highlands, *J. Geophys. Res.*, *108*(E7), 5069, doi:10.1029/2002JE002013.

Head, J. W., and T. B. McCord (1978), Imbrian-age highland volcanism on the Moon: The Gruithuisen and Mairan domes, *Science*, *199*, 1433–1436, doi:10.1126/science.199.4336.1433.

Jolliff, B. L. (1998), Large-scale separation of K-frac and REEP-frac in the source regions of Apollo impact-melt breccias and a revised estimate of the KREEP composition, *Int. Geol. Rev.*, *40*, 916–935, doi:10.1080/00206819809465245.

Jolliff, B. L., C. Floss, I. S. McCallum, and J. M. Schwartz (1999), Geochemistry, petrology, and cooling history of 14161,7373: A plutonic lunar sample with textural evidence of granitic-fraction separation by silicate-liquid immiscibility, *Am. Mineral.*, *84*, 821–837.

Jolliff, B. L., et al. (2011), Compton-Belkovich: Non-mare silicic volcanism on the Moon's far side, *Nat. Geosci.*, *4*, 566–571, doi:10.1038/ngeo1212.

Korotev, R. L. (1998), Concentrations of radioactive elements in lunar materials, *J. Geophys. Res.*, *103*, 1691–1701, doi:10.1029/97JE03267.

Lawrence, D. J., R. C. Elphic, W. C. Feldman, T. H. Prettyman, O. Gasnault, and S. Maurice (2003), Small-area thorium features on the lunar surface, *J. Geophys. Res.*, *108*(E9), 5102, doi:10.1029/2003JE002050.

Lawrence, D. J., B. R. Hawke, J. J. Hagerty, R. C. Elphic, W. C. Feldman, T. H. Prettyman, and D. T. Vaniman (2005), Evidence for a high-Th evolved lithology on the Moon at Hansteen Alpha, *Geophys. Res. Lett.*, *32*, L07201, doi:10.1029/2004GL022022.

Lucey, P. G., D. T. Blewett, and B. L. Jolliff (2000), Lunar iron and titanium abundance algorithms based on final processing Clementine ultraviolet visible images, *J. Geophys. Res.*, *105*(E8), 20,297–20,305, doi:10.1029/1999JE001117.

Matsunaga, T., et al. (2008), Discoveries on the lithology of lunar crater central peaks by SELENE Spectral Profiler, *Geophys. Res. Lett.*, *35*, L23201, doi:10.1029/2008GL035868.

Papike, J. J., G. Ryder, and C. K. Shearer (1998), Lunar samples, *Rev. Mineral.*, *36*, 1–189.

Robinson, K. L., and G. J. Taylor (2011), Intrusive and extrusive lunar felsites, *Lunar Planet. Sci.*, *XLII*, Abstract 1257.

Robinson, M. S., et al. (2010), Lunar Reconnaissance Orbiter Camera (LROC) instrument overview, *Space Sci. Rev.*, *150*, 81–124, doi:10.1007/s11214-010-9634-2.

Scholten, F., et al. (2010), Towards global lunar topography using LROC WAC stereo data, *Lunar Planet. Sci.*, *XLI*, Abstract 2111.

Scott, D. H., and R. E. Eggleton (1973), Geologic map of the Rumker quadrangle of the Moon, *U.S. Geol. Surv. Misc. Invest. Ser. Map*, *I-805*.

Tran, T., et al. (2011), Morphometry of lunar volcanic domes from LROC, *Lunar Planet. Sci.*, *XLII*, Abstract 2228.

Wilson, L., and J. W. Head (2003), Lunar Gruithuisen and Mairan domes: Rheology and mode of emplacement, *J. Geophys. Res.*, *108*(E2), 5012, doi:10.1029/2002JE001909.

J. A. Arnold and T. D. Glotch, Department of Geological Sciences, Stony Brook University, Stony Brook, NY 11794-2100, USA. (tglotch@notes.cc.sunysb.edu)

T. A. Giguere, B. R. Hawke, and P. G. Lucey, Hawaii Institute of Geophysics and Planetology, University of Hawaii at Manoa, Honolulu, HI 96822, USA.

J. J. Hagerty, Astrogeology Science Center, U.S. Geological Survey, Flagstaff, AZ 86001, USA.

B. L. Jolliff, Department of Earth and Planetary Sciences, Washington University in St. Louis, St. Louis, MO 63130, USA.

D. A. Paige and J.-P. Williams, Department of Earth and Space Sciences, University of California, Los Angeles, CA 90095-1567, USA.